

In vitro and in silico characterization of angiogenic inhibitors from *Sophora interrupta*

Pardhasaradhi Mathi^{1,2} · Ganesh Kumar Veeramachaneni¹ · K. Kranthi Raj¹ · Venkateswara Rao Talluri¹ · Venkata Raman Bokka³ · Mahendran Botlagunta¹

Received: 5 February 2015 / Accepted: 1 September 2016 / Published online: 28 September 2016
© Springer-Verlag Berlin Heidelberg 2016

Abstract *Sophora interrupta* Bedd, (Fabaceae) is used in Indian folk medicine to treat cancer. Angiogenesis is one of the crucial characteristics of cancer metastasis and is regulated by vascular endothelial growth factor (VEGF). In this study, we examined the antiangiogenic properties of the root ethyl acetate extract of *Sophora interrupta* by various methods. In vitro antioxidant activity (100–600 µg/ml) of *S. interrupta* ethyl acetate (SEA) extract was evaluated by DPPH and ABTS, anti-inflammatory activity (50, 100 and 150 µg/ml) by estimating nitric oxide (NO) levels, anti-angiogenic activity (200 and 500 µg/ml) was validated by chorio allantoic membrane (CAM) assay and in silico molecular dynamic (MD) simulations analyses (25 ns) were performed to identify the anti-angiogenic compounds extracted from root extract. The antioxidative activity of SEA extract at IC₅₀ (200 ± 0.6 µg/mL) is equal to that of ascorbic acid at IC₅₀ (50 ± 0.6 µg/mL), and the anti-inflammatory activity of SEA

extract at IC₅₀ (150 ± 0.2 µg/mL) was inhibited significantly by nitric oxide (NO) production. The SEA extract significantly reduced the sprouting of new blood vessels at ID₅₀ 500 ± 0.13 µg/mL in the CAM assay. Gas chromatography–mass spectrometry analysis of the SEA extract detected 34 secondary metabolites, of which 6a,12a-dihydro-6H-(1,3)dioxolo(5,6)benzofuro(3,2-c)chromen-3-ol (maackiain) and funiculosin formed strong hydrogen bond interactions with Lys 920, Thr 916 and Cys 919 (2H), as well as Glu 917 of VEGFR2, and these interactions were similar to those of the anti-angiogenic compound axitinib. Significant findings in all the assays performed indicate that SEA extract has potential anti-angiogenic compounds that may interfere with VEGF-induced cancer malignancy.

Keywords Fabaceae · Angiogenesis · Mass spectroscopy · Molecular dynamic simulations

Electronic supplementary material The online version of this article (doi:10.1007/s00894-016-3102-1) contains supplementary material, which is available to authorized users.

✉ Mahendran Botlagunta
bmnchowdary@gmail.com

¹ Biomedical Research Laboratory, Department of Biotechnology, KLEF University (Koneru Lakshmaiah Educational Foundation), Green fields; Vaddeswaram, Guntur (Dist) 522502, Andhra Pradesh, India

² Upstream Process Development Team, Lupin Limited, Biotechnology R&D, 1156, Ghotawade Village, Mulshi Taluka Pune-411042, India

³ Department of Basic Sciences-Chemistry, Madanapalle Institute of Technology and Science (MITS), Madanapalle, Chittoor 517325, Andhra Pradesh, India

Introduction

Angiogenesis is the action of contemporary blood vessels growing from preceding capillaries and post-capillary venules [1]. It occurs in several physiological and pathological circumstances, such as during embryonic development and wound healing, as well as in patients with chronic inflammatory diseases and various metastatic tumor growths [2]. The process of angiogenesis is regulated mainly by vascular endothelial growth factor (VEGF)—a secretory dimeric glycoprotein of approximately 40 kDa. The VEGF family comprises five members: VEGF-A, -B, -C, and -D and placenta growth factor (PGF). VEGF-A was found to be an important regulatory factor for both vasculogenesis and angiogenesis through the stimulation of various cells, including leukocytes

and endothelial cells [3]. When VEGF binds to tyrosine kinase receptors (R1 and R2) on the cell surface, homodimers formed through transphosphorylation stimulate a variety of cellular responses ranging from generating signal outputs to the recruitment and proliferation of endothelial cells. Hence, the triggered development of angiogenesis can be seen in this process. Generally, VEGF expression levels in serum are below the level of detection. The enhanced expression of VEGF leads to several vascular diseases, such as bronchial asthma, diabetes mellitus, diabetic retinopathy, rheumatoid arthritis, angiosarcoma, preeclampsia, and cancer [4]. Therefore, for such diseases, it is essential to regulate the expression of VEGFs using inhibitors to reduce angiogenesis. Several inhibitors, such as apigenin, bevacizumab (Avastin), sunitinib (Sutent), sorafenib (Nexavar), axitinib (Inlyta), and pazopanib (Votrient), are used to treat VEGF-associated pathologies like cancer [5]; however, they have been shown to cause several side effects in humans including the impairment of digestive and neurological functions [6]. Despite the known side effects, these drugs are still used for their anticancer activity. From among these drugs, we have chosen axitinib as a standard drug with which to identify the similar structural, functional activity relationship from secondary metabolites of *Sophora interrupta*.

Axitinib has been shown to exhibit anticancer properties by downregulating the production of HIF-1 α and VEGF [7]. Recent focus has shifted from traditional treatments to the target-specific inhibition of VEGF with low side effects [8] and identifying natural products that downregulate expression of VEGF. In the continuing effort to identify medicinal plants against cancer, one widely distributed medicinal plant *S. interrupta* Bedd, is used to treat the VEGF-associated disorders. *S. interrupta* is a woody perennial shrub, and species of this genus are distributed widely across the globe. It has been shown to possess various pharmacological properties, including antioxidant [9], anticancer [10], anti-asthmatic, antineoplastic, antimicrobial [11], antiviral, antidote, antipyretic, cardiogenic, anti-inflammatory and diuretic activities. It has also been used in the treatment of skin diseases such as eczema, colitis and psoriasis [12]. The methanol extract from the leaves of *S. interrupta* (MESI) significantly inhibited tumor volumes and enhanced the survival rates of mice with Dalton's ascitic lymphoma (DAL), and it does not affect the hemoglobin content in red blood cell (RBC) and white blood cell (WBC) counts [13]. On the other hand, it was shown recently that *Sophora flavescens* exhibits anti-angiogenesis activity by decreasing the expression of VEGF [14]. Thus it will be interesting to identify secondary metabolites from the same family and their anti-angiogenic activities against cancer. In the present study, we studied the inflammatory and angiogenic activity of *S. interrupta* ethyl acetate (SEA) root extract in vitro, and validated results via in silico approaches.

Materials and methods

Chemicals, materials and software

Ethyl acetate (EtOAc) solvent was purchased from Merck Millipore (Mumbai, India); DPPH (1, 1-diphenyl-2-picrylhydrazyl hydrate) was purchased from Hi-Media (Mumbai, India). Fertilized chicken eggs were obtained from local vendors. Cisplatin was purchased from KEMOPLAT, Fresenius Kabi; Batch no: 881FP009. The Schrödinger Maestro, Desmond software systems were used for docking and molecular dynamics (MD) studies and AngioQuant Toolbox, MATLAB 6.5 software was used to quantify blood vessels. All other chemicals used in the study were analytical grade products.

Methods

Measuring antioxidants by DPPH and ABTS assay

The radical scavenging potential of the SEA extract was determined against free radical DPPH and ABTS standard protocols [15]. Various concentrations of extract (100, 200, 300, 400, 500 and 600 $\mu\text{g}/\text{mL}$) were added to the DPPH methanol stock solution (100 μM) and 2 mL of ABTS radical cation solution (2 mM), respectively. The samples were incubated for 15 min at room temperature and the color change from deep violet to light yellow for DPPH, and blue color to colorless for ABTS, was observed. Absorbance was measured at 517 nm and 734 nm, respectively, against a blank using a UV-vis spectrophotometer (DYNAMICA Halo DB20; Australia). Ascorbic acid was used as a standard antioxidant (1 mg/mL). All experiments were carried out in triplicate, and the results represented as mean \pm SD. The percentage of free radical scavenging is determined by the following expression:

Percentage (%) Free radical scavenging

$$= \frac{(\text{OD of Control}) - (\text{OD of test})}{(\text{OD of Control})} \times 100$$

where, OD is optical density. IC₅₀ values were calculated using linear regression analysis. The IC₅₀ values signify the concentration of the sample that can scavenge 50 % of the DPPH and ABTS free radicals.

Anti-inflammatory activity on RAW 264.7 cell lines

The macrophage (RAW 264.7) cell line was initially established from a tumor induced in Balb/c mice by Abelson murine leukemia virus [16]; these cells were maintained in DMEM with 10 % heat-inactivated FBS, 100 U/mL penicillin, and 100 mg/mL streptomycin and incubated in 5 % CO₂ at 37 °C. The RAW 264.7 cells are semi-adherent; while a few

cells grow in suspension, some cells loosely adhere to the surface and others flatten out and attach to the flask. Extract dissolved in DMSO was added to cells at final concentrations of 50, 100 and 150 $\mu\text{g/mL}$ in the presence and absence of yeast (5×10^7 cells/mL) for 24 h. The final concentration of DMSO was adjusted to $\leq 0.1\%$ of all treatments.

Nitric oxide assay by Griess reagent

Nitric oxide (NO) yield was ascertained by quantifying the amount of nitrite accumulation in the culture supernatant by Griess reagent [17]. Briefly, RAW 264.7 cells (1×10^5 cells/well) were seeded in 96-well plates and incubated for 6 h. Cells were treated in the presence and absence of yeast (5×10^7 cells/mL) at various concentrations of the SEA extract for 24 h, and then 100 μL culture supernatant from each sample was combined with 50 μL Griess reagent and incubated at 37 °C for 10 min. The optical density was read at 550 nm on a plate reader. The NO concentration was determined using dilutions of sodium nitrite (NaNO_2) as standard.

Anti-angiogenesis activity using chorio allantoic membrane

The ability of the SEA extract to inhibit angiogenesis was determined using a modified chorio allantoic membrane (CAM) assay as described by Foubert et al. [18]. Fertilized eggs on day 1 were purchased from the local vendors, shell surface disinfected using 70 % ethanol, and transferred to an incubator (GENEI, Bangalore, India) at 37 °C with 75 % humidity to provide optimal growth conditions. For equal distribution of blood vessels, the eggs were turned over twice a day. On day 8, the eggs were again disinfected with ethanol (70 %), and a square shaped window of 1 cm^2 was opened in the eggshell with a saw blade, exposing the white inner shell membrane. The plant extract was dissolved in (DMSO) at variable concentrations and applied to a sterile Whatman membrane sheet. The extract was air dried on a disinfected surface, and implanted on the outer one-third of the growing CAM blood vessels. Controls were treated with blank DMSO discs. The distinct allantoic blood vessels around the DMSO discs were examined 15 min and 30 min after implantation. The angiogenic responses were captured using a high resolution (Nikon, Tokyo, Japan) camera. The images were imported into *AngioQuant* software to score the number, size, and length of the blood vessels. Black and white skeleton pruned images were generated corresponding to the corrected color images. The intensity of individual vessels was quantified by densitometry using *AngioQuant* software [19]. Values represented total length and size of tubules as well as mean length and size of tubules corresponding to the kernel size 1, segment not to remove edge tubules, prune size 10 according to *AngioQuant* software. The results are presented as a mean percentage of inhibition compared to the control \pm SD, ($n = 3$).

Gas chromatography–mass spectrometry separation conditions

Gas chromatography–mass spectrometry (GC-MS) analysis of EtOAc extract was performed using a GC-MS-QP 2010 (SHIMADZU, Kyoto, Japan) equipped with electron impact (EI) mode (ionizing potential -70 eV) as well as a capillary column (VF-5 ms) (length 30 m \times diameter 0.25 mm, film thickness 0.25 μm) packed with 5 % phenyl dimethyl silicone. The ion source temperature was maintained at 240 °C, and helium was utilized as a carrier gas with 99.99 % purity. Samples were injected at a temperature of approximately 240 °C with a split ratio of 10:1 and a flow rate of 1.51 ml/min. A mass analyzer was used in full scan mode from 45 m/z to 1000 m/z, with a total MS running time of 36 min; electron impact ionization was used at 70 eV.

Identification of phyto-constituents

The interpretation of phytoconstituents obtained from GC-MS analysis were compared with those available in the in-house mass spectral library (NIST-2005). The molecular mass, name and structure of the components in the extract were determined.

Protein and ligand preparation

The 3D protein structural coordinates of VEGFR1 (PDB ID: 3HNG) and VEGFR2 (PDB ID: 3U6J) with a resolution of 2.7 Å and 2.15 Å, were retrieved from PDB [20]. A protein preparation wizard in the Schrödinger suite, version 9.6, [21] was used to prepare the proteins by adding hydrogens, optimizing and minimizing with force field OPLS 2005 [22]. The *S. interrupta* plant metabolites and compounds characterized through GC-MS were sketched using Chembiosuite [23]. The chemical structures of all compounds were imported into the Schrödinger Maestro suite and further prepared using the Lig Prep module, version 2.6 [24]. Lig Prep module was used to neutralize, desalt, correct the Lewis structure and check for metal binding sites. “Retain the specified chiralities” option was chosen as stereo isomers are not accessible; 3D geometries of all ligands were minimized using an OPLS 2005 force field.

Molecular docking

GLIDE module version 6.1 in the Schrödinger suite, a grid-based ligand docking method with energetics, was used for ligand docking [25]. A grid box with the size 72 Å \times 72 Å \times 72 Å with coordinates X = 12.188, Y = 20.152, and Z = 48.922 were generated at the centroid of the crystal ligand, as the grid based protocol requires a grid for ligand docking [26]. Using the Extra precision (XP) mode in the ligand docking protocol [27] the prepared metabolites (ligands) were

docked into the active pockets of VEGFR1 and VEGFR2. The ligands were ranked and the interactions between amino acids of protein and ligand were analyzed based on the G-scores. The interactions were depicted using Ligplots [28]. Top ranked molecules were further analyzed using molecular dynamic (MD) simulations.

Molecular dynamic simulations

All MD simulations to study the stability of protein–ligand complexes were performed with Desmond version 2013 [29]. In the present study, prepared protein–ligand complex was subjected to the TIP4P water model in an orthorhombic periodic boundary box of size 376,702 Å for 3HNG complexes and 440,055 Å for 3U6J complexes under solvated conditions using the system builder. To neutralize the system, three Cl⁻ ions were added based on the total charge of the system, and also a salt concentration of 0.15 M was added to maintain the charge of the complex. After building the prepared model system, the total number of atoms present in the built system was calculated, and the system was minimized up to a maximum of 5000 iterations. Further MD simulations studies were carried out with a periodic boundary condition in NPT ensemble, temperature at 300 K, 1 atmospheric pressure, and the model was relaxed using the default relaxation protocol integrated in Desmond. The simulation was carried out on all the VEGFR1 and VEGFR2 complexes along with a standard over a time period of 25,000 ps at 5-ps intervals, and a time step of 5 ps. The final trajectory file was taken for calculating the RMSD, RMSF and total energy of the complexes.

Statistical analysis

All results are expressed as mean \pm SD, and significant differences between the treatment and control groups were evaluated by one-way analysis of variance (ANOVA); differences were considered significant at $P < 0.05$.

Results

Antioxidant (DPPH and ABTS) activity of SEA extract

To investigate the antioxidant activity of root extract, roots were collected, washed twice, milled to a fine powder that was then soaked in EtOAc solvent for 48 h. The resulting crude extract was tested for the presence and absence of phytochemicals (Fig. S1). The values obtained for antioxidant assays are represented as percentages of free radical scavenging activities at various concentrations, as given in Fig. 1. The results revealed dose-dependent inhibition of DPPH and ABTS scavenging activity at increasing concentrations of SEA extract (Fig. 1a, c). Interestingly, a 2-fold change in the

inhibitory activity of SEA extract against DPPH was noticed at 500 $\mu\text{g/mL}$, when compared with the 400 $\mu\text{g/mL}$ concentration. According to these data, $500 \pm 0.13 \mu\text{g/mL}$ and $400 \pm 0.11 \mu\text{g/mL}$ SEA extract was required for 50 % inhibition of DPPH and ABTS activity, respectively. We used the well-known antioxidant ascorbic acid (5–50 $\mu\text{g/mL}$) as a standard. The 20 % DPPH and 75 % ABTS scavenging activity by SEA extract at $200 \pm 0.6 \mu\text{g/mL}$ and $500 \pm 0.13 \mu\text{g/mL}$ was similar to that of ascorbic acid at $50 \pm 0.5 \mu\text{g/mL}$ concentration (Fig. 1b,d). The higher percentage of ABTS scavenging activity was due to the fact that the antioxidants of aromatic plants scavenge the cation radical ABTS⁺ more effectively than DPPH⁺. Overall, these results suggest that SEA extract contains bioactive phytochemical constituents with potential antioxidant activity.

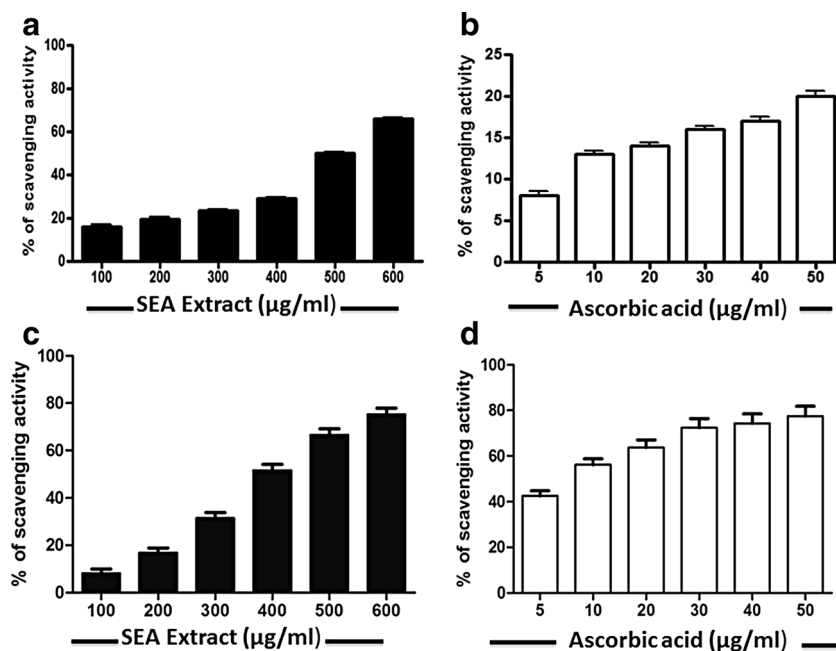
Anti-inflammatory effects of SEA extract on *Candida albicans*-induced RAW 264.7 cells

The RAW 264.7 cells were washed and morphological changes captured using an optical inverted microscope (Fig. 2a–c). Untreated cells showed an elongated smooth form of spreading whereas *Candida*-induced cells showed an irregular and rough form of spreading. But no measurable cell death was noticed, which was evident from the percentage of cell viability as compared to untreated cells (Fig. 2d). On contrary, SEA extract treated cells showed variant intermediate morphology compared to untreated cells. NO production was used as an index of inflammation [17], and the production of NO was seen across all samples. As shown in Fig. 2e, *Candida*-treated cells showed 100 % production of NO, whereas SEA extract-treated cells significantly inhibited *Candida*-stimulated NO production in a dose-dependent manner and the concentration of NO ($150 \pm 0.81 \mu\text{g/mL}$) was similar to that of control cells, reporting an IC₅₀ $50 \pm 0.35 \mu\text{g/mL}$. It was concluded that SEA extract can inhibit inflammatory *Candida*-mediated cell injury.

CAM assay for anti-angiogenesis activity

An in ovo CAM assay was performed to confirm the anti-angiogenic activity of SEA extract. As represented in Fig. 3a, applying SEA extract on blood vessels resulted in less thickness without bulging appearance, reflecting an anti-angiogenic activity that was similar to that of cisplatin, a positive control. Moreover, SEA extract effectively inhibited angiogenesis in a time- and dose-dependent manner in the chick embryo model. The length and size of the blood vessels was calculated using AngioQuant software [19]. As depicted in Fig. 3b, the length and size of the blood vessels decreased gradually in dose-dependent manner. At ID₅₀ $500 \pm 0.13 \mu\text{g/mL}$, the number of vessels was reduced (2-fold decrease) to half compared to the control. Overall, these results suggest that SEA extract inhibits

Fig. 1a–d Determination of DPPH and ABTS free radical scavenging activities of *Sophora interrupta* ethyl acetate (SEA) extract at different extract concentrations. **a, b** DPPH scavenging activity of SEA extract (**a**) and standard ascorbic acid (**b**) ($\mu\text{g/ml}$). **c, d** ABTS radical cation scavenging activity of SEA extract (**c**) and standard ascorbic acid (**d**) ($\mu\text{g/ml}$)



sprouting of new blood vessels from chicken aorta, and microvessel formation in the CAM model.

GC-MS analysis of SEA extract

The powdered root of the *S. interrupta* plant was carefully macerated in the presence of EtOAc. Excess EtOAc removed by a simple distillation technique, and the finalized form of the crystalline powder was analyzed by GC-MS analysis. The spectrum profile of the GC-MS data of the *Sophora* were compared with the mass spectrum of known components stored in the

National Institute of Standards and Technology (NIST) library [30]. Thirty-four compounds were identified in SEA extract, which is evident from the GC-MS chromatogram (Table S1).

Docking studies

The plant-derived molecules were docked into the active pocket of VEGFR1 and VEGFR2; the lead molecules along with the standard axitinib are listed in Table 1, and the remaining molecules in Table S2. Out of 34 metabolites, only 1 (maackiain) showed a higher G-score (-7.8) than axitinib.

Fig. 2a–e In vitro anti-inflammatory activity of SEA extract using RAW264.7 macrophage cell lines. Images showing phenotypic characteristics of RAW cells. **a** Control. **b** Yeast-induced inflammation. **c** SEA extract treated RAW264.7 cells. **d** Percentage of cell viability. **e** Nitric oxide (NO) concentration at various concentrations of SEA extract

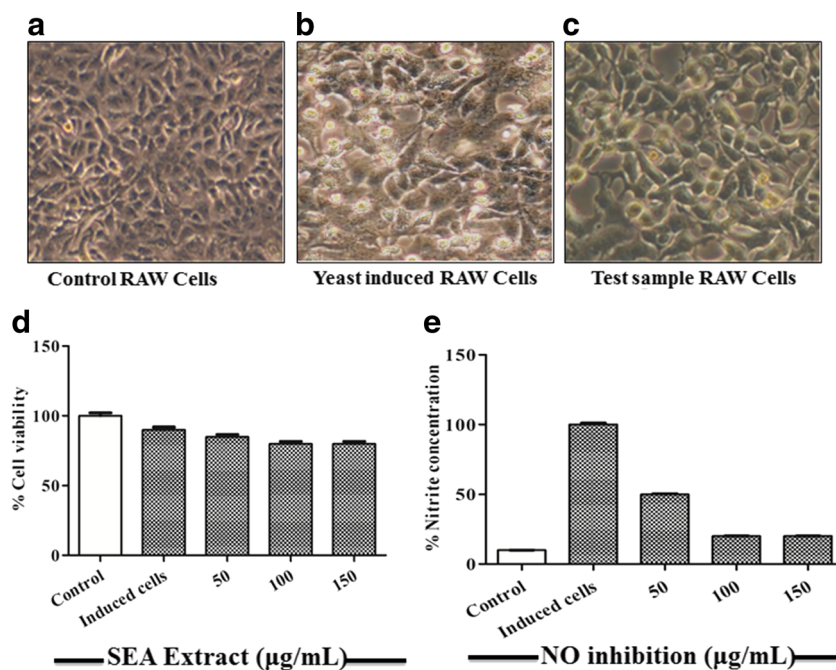
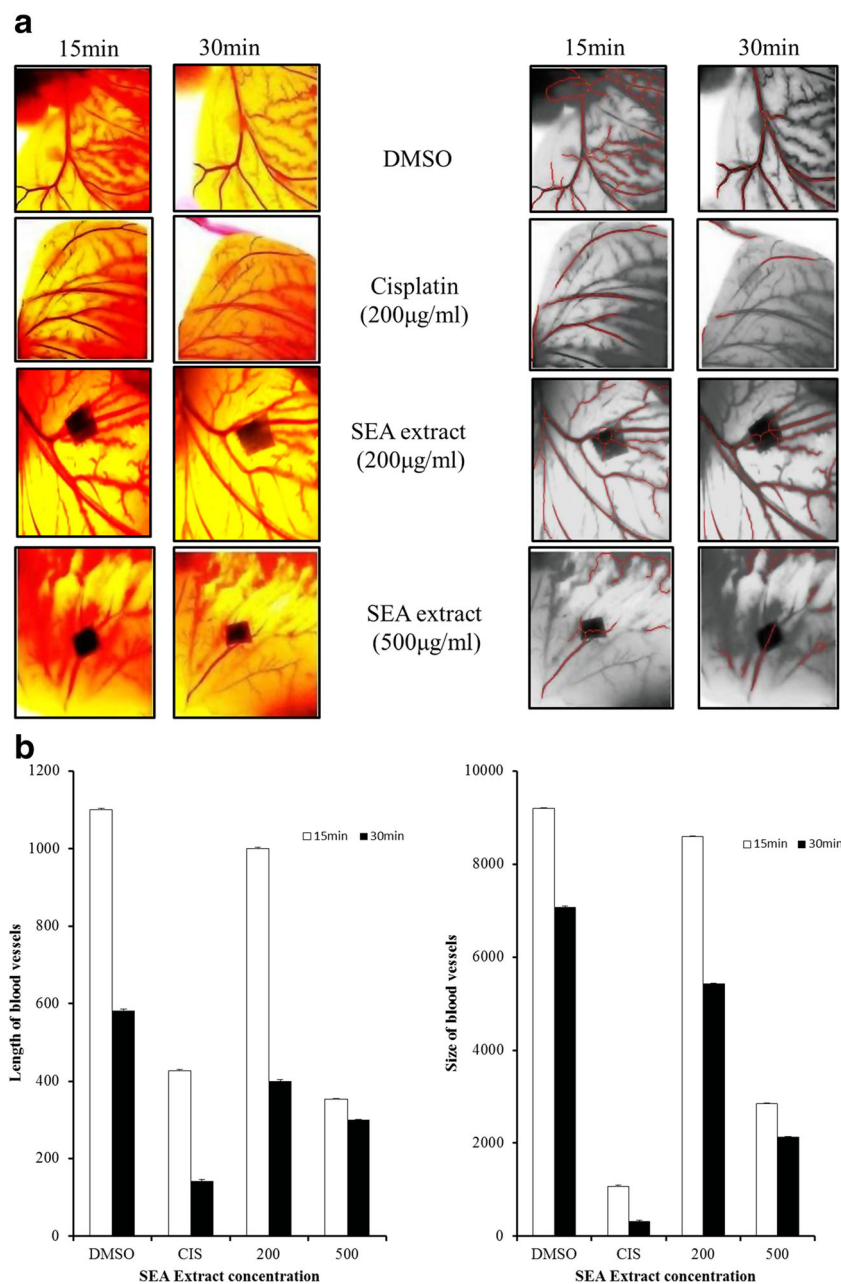


Fig. 3a,b Effect of SEA extract on chorio allantoic membrane (CAM). **a** *Left panel* Effect of SEA extract on CAM at 200 $\mu\text{g/ml}$ and 500 $\mu\text{g/ml}$ concentrations with time, *right panel* (grey images) Software (AngioQuant)-generated blood vessel densities in CAM. **b** Graphs depicting the length (*left*) and size (*right*) of blood vessels. $n = 3$, mean \pm SD



Maackiain formed a single hydrogen bond (H-bond) with the active site residue Asp 1040 ($\text{O}\cdots\text{HO}$ 2.25 Å) and a π - π stacking with Phe 1041 residue of the receptor. The binding energy between the VEGFR1 and maackiain showed

$-13.6 \text{ K cal mol}^{-1}$. Standard inhibitor axitinib was initially docked in both receptors for analyzing the important residues present inside the active pocket. Axitinib formed H-bonds with Glu 878 ($\text{HN}\cdots\text{O}$ 1.91 Å), Asp 1040 ($\text{O}\cdots\text{H}$ 2.22 Å),

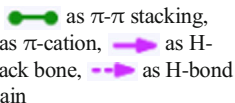



Table 1 Predicted Glide scores for the binding of maackiain, funiculosin and axitinib to vascular endothelial growth factor (VEGF) R1 and R2

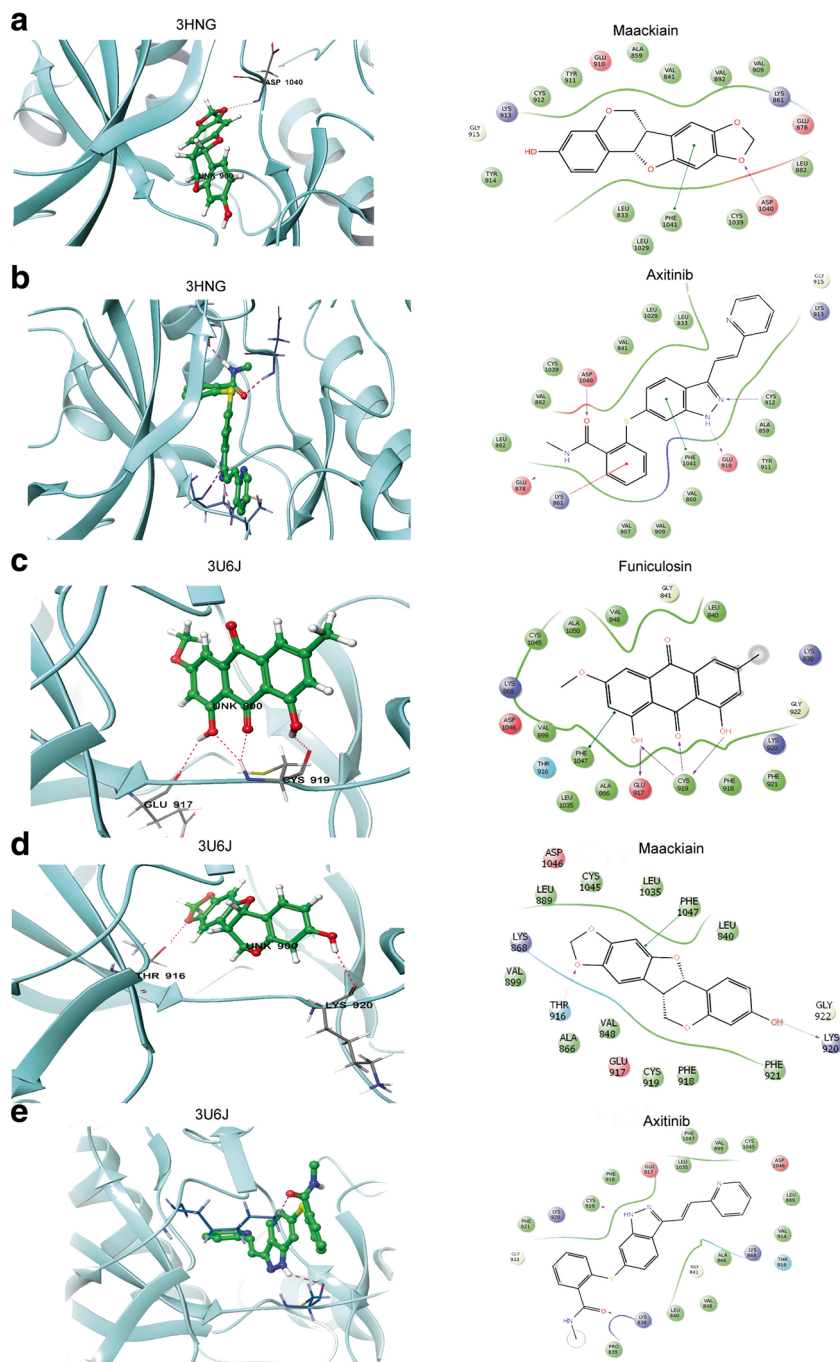
Protein	Compounds	G-Score	Ligand interactions
VEGFR1	Axitinib	-14.2	Glu 910, Glu 878, Cys 912, Asp1040
	Maackiain	-7.8	Asp 1040 (H-bond), Phe 1041(π - π)
VEGFR2	Axitinib	-7.9	Cys 919 (H-bond), Lys 838
	Funiculosin	-9.4	Cys 919 (3 H-bonds),Glu 917 (H-bond), Phe 1047(π - π)
	Maackiain	-8.5	Thr 916 (H-bond), Lys 920 (H-bond), Phe 1047(π - π)

Glu 910 (HN \cdots O 2.18 Å) and Cys 912 (N \cdots H 1.88 Å) amino acids of the VEGFR1 receptor. Also, a π - π stacking with Phe 1041 and a π -cation interaction with Lys 861 were observed in the VEGFR1-axitinib complex. The energy and G-score of the complex was -83.3 kcal mol $^{-1}$ and -14.2 kcal mol $^{-1}$, respectively (Fig. 4).

In VEGFR2, of the 34 metabolites tested, funiculosin and maackiain exhibited the highest G-scores compared with Axitinib. Funiculosin interacted with Cys 919 (HO \cdots SH 1.99 Å; O \cdots SH 1.94 Å; HO \cdots SH 2.43 Å), Glu 917 (HO \cdots O

2.06 Å) via four H-bonds and one π - π stacking with Phe 1047. The binding energy of the complex was -39.2 kcal mol $^{-1}$ and the G-score was -9.4 kcal mol $^{-1}$. Another VEGFR2-maackiain complex displayed two H-bonds and one π - π interaction. H-bond interactions were observed with Thr 916 (O \cdots HO 1.95 Å) and Lys 920 (HO \cdots O 1.82 Å). Active pocket residue Phe 1047 showed π - π stacking with the maackiain molecule. Energy and G-score of the complex were -34.9 kcal mol $^{-1}$ and -8.5 kcal mol $^{-1}$, respectively. In the VEGFR2-axitinib complex, axitinib formed two H-bonds. One H-bond was observed

Fig. 4a-e Binding poses and Ligplots panel of active molecules. **a** 3D and 2D orientation of Axitinib in the binding pocket of VEGFR1. **b** 3D and 2D orientation of Maackiain in the binding pocket of VEGFR1. **c** 3D and 2D orientation of Axitinib in the binding pocket of VEGFR2. **d** 3D and 2D orientation of Funiculosin in the binding pocket of VEGFR2. **e** 3D and 2D orientation of Maackiain in the binding pocket of VEGFR2. The proteins are displayed in *green ribbon* and ligand molecules are in *yellow ball and stick* notation. The interacting residues are labeled and shown in different colors.  as π - π stacking,  as π -cation,  as H-bond backbone,  as H-bond side chain



with Lys 838 (O \cdots NH 2.11 Å) and another with Cys 919 (HN \cdots O 2.41 Å). The binding affinity of the VEGFR2-axitinib complex showed energy and G-scores of -74.3 kcal mol $^{-1}$ and -7.9 kcal mol $^{-1}$, respectively.

The docking results show that three compounds can act as a potential anti-angiogenic leads; therefore, an *in silico* ADME parameter screening study was performed using QikProp v3.5. Axitinib, maackiain and funiculosin were calculated with standard parameters of ADME (Table 2). The ADME results revealed no violations in their physiochemical properties except for an aqueous solubility parameter—a common factor that can be rectified by techniques such as particle size reduction, salt formation, solid dispersion, use of surfactants, complexation etc. [31]. One more point to be noted was that this parameter for these molecules was far better than the standard.

Molecular dynamic simulations

The ligand–protein complexes were subjected to MD simulations for 25,000 ps using the Desmond module. Van der Waal forces, hydrogen bondings, π – π and π –cation interactions play an important role in maintaining the stability of protein–ligand complexes. The interactions in VEGFR1 and VEGFR2 complexes with ligands were monitored for consistency throughout the simulation time interval. The H-bond interactions of receptor and ligand complexes before and after simulations are reported in Table 3.

Simulation analysis of VEGFR1

The total energy of the VEGFR1–maackiain and –axitinib complexes was stable; that of the R1–maackiain complex was between -130 kcal mol $^{-1}$ and -140 kcal mol $^{-1}$, and for the R1–axitinib complex it was between -220 kcal mol $^{-1}$ and -230 kcal mol $^{-1}$ throughout the simulation (Fig. S2a,b). The RMSD scale for VEGFR1 with maackiain started initially at 0.0 Å; a deviation of 2.5 Å was observed from 10 ps to 10,000 ps, and stability was then sustained until 25,000 ps,

with an RMSD between 2.0 Å and 3.0 Å, and no deviations were noted in the last picoseconds of the simulations. Axitinib RMSD started initially at 0.0 Å, rose to 2.0 Å at 2000 ps and sustained stability throughout the simulations (Fig. 5a). The RMSF of amino acids in VEGFR1 in the presence of maackiain was below 4.0 Å, and for axitinib it was below 3.5 Å. Maackiain exhibited 31 % and 30 % H-bond formation with Lys 861 and Cys 912 of VEGFR1. Axitinib showed 99 % H-bonds formation with Glu 910 and Glu 878, 87 % and 83 % of H-bonds were also formed with Asp 1040 and Cys 912 of VEGFR1 (Fig. 6a).

Simulation analysis of VEGFR2

The total energy of VEGFR2–Funiculosin, R2–maackiain and R2–axitinib interactions were between -235 and -240 kcal mol $^{-1}$, -135 kcal mol $^{-1}$ and -140 kcal mol $^{-1}$, and -220 kcal mol $^{-1}$ and -230 kcal mol $^{-1}$ throughout the simulation (Fig. S3a–c). The deviations in R2–funiculosin were between 2.0 Å and 2.5 Å throughout the molecular simulations. Minimum deviations around 2.5 Å were observed between the 5000 ps and 21,000 ps intervals. The natural compound maackiain showed an initial RMSD at 1.2 Å with the VEGFR2 binding pocket, reaching 2.5 Å at 2000 ps and sustaining stability until the last frame. The deviations in the VEGFR2–axitinib complex were maintained between 0.0 Å and 2.5 Å. Stability was obtained after 2000 ps and stability sustained until the last frame. The deviations for the VEGFR2 complexes are depicted in Fig. 5b. The RMSF of amino acids in VEGFR2 in the presence of funiculosin and maackiain were below 3.5 Å, and that of axitinib was below 2.5 Å. The hydrogen interaction percentage of the VEGFR2–funiculosin complex was 99 % and 94 % with Glu 917 and Cys 919. Another metabolite, maackiain, showed 38 % interactions with Cys 919 active amino acid residue of VEGFR2. The VEGFR2–axitinib complex showed similar bonding of 83 % and 43 % of H-bonds with Cys 919 and Asn 923. The interaction percentages of VEGFR2 complexes are illustrated in Fig. 6b.

Table 2 Predicted ADME properties (QikProp 2.3 module) of lead compounds

Compound	QPlogPo/w ^a	QPlogS ^b	QPPCaco ^c	QPPMDCK ^d	Percent human oral absorption ^e
Axitinib	4.585	−6.196	602.586	382.726	100
Maackiain	2.586	−3.063	3003.556	1624.118	100
Funiculosin	1.847	−3.034	265.626	118.047	81.084

^a Predicted octanol/water partition coefficient (recommended range -2.0 to 6.5)

^b Predicted aqueous solubility, log S. S in mol/dm 3 in the concentration of the solute in a saturated solution that is in equilibrium with the crystalline solid (recommended range -2.0 to 6.5)

^c Predicted apparent Caco-2 cell permeability in nm/sec (recommended range <25 poor to >500 great)

^d Predicted apparent MDCK cell permeability in nm/sec (recommended range <25 poor to >500 great)

^e Percentage of human oral absorption (recommended range <25 % poor to >80 % high)

Table 3 Percentage of hydrogen (H)-bond interaction between active amino acid residues of protein and ligands. MD Molecular dynamic simulation

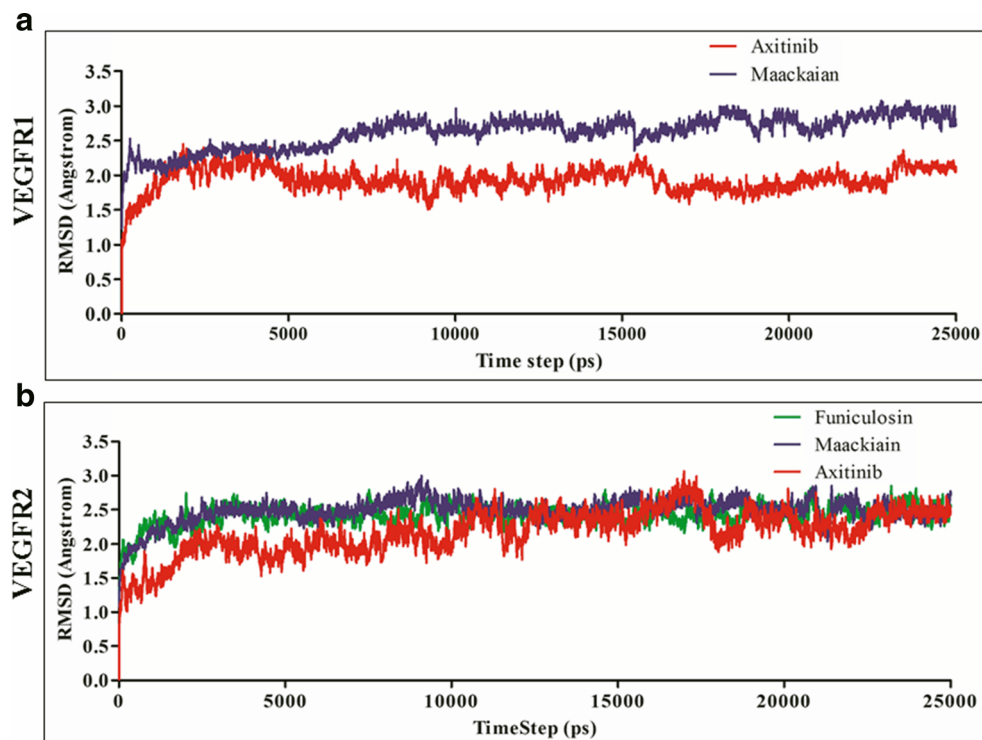
Protein	Aminoacids interactions		H-bond formation
	Before MD	After MD	Before/after MD
VEGFR1			
Axitinib	Cys 912; Glu 910;	Cys912; Glu 910;	2 / 2
	Asp 1040; Glu 878	Asp 1040; Glu 878	1 / 2
Maackiaian	Asp 1040	Lys861; Cys912	
VEGFR2			
Axitinib	Cys 919; Lys 838	Cys919; Asn 923	2 / 2
Funiculosin	Glu 917; Cys 919	Glu 917; Cys 919	4 / 4
Maackiaian	Thr916; Lys920	Cys919	2 / 1

Discussion

S. interrupta belongs to the family of Fabaceae. Species in this family are distributed across the world, and have been shown to have many pharmacological actions [32]. The results of *S. interrupta* phytochemical analysis demonstrate that SEA extract is not only positive for terpenoids and alkaloids, but also showed a significant antioxidant and anti-inflammatory activity. Free radicals are noted for their vital role in pathological manifestations. The antioxidants from SEA extract scavenge free radicals like DPPH and ABTS, and the degree of discoloration indicates the scavenging potency of the plant extract. In the present study, 200 µg/mL and 500 µg/mL concentrations had the capacity to neutralize DPPH and ABTS, respectively. The antioxidant and anti-inflammatory potential of

phytoconstituents has been shown to reduce the risk of blood vessel-associated cancer [33]. NO has been implicated in many conditions such as inflammation and carcinogenesis [34]. Overproduction of NO during inflammation is a target for the development of new therapeutic molecules. Thus, inhibitors from SEA extract significantly suppressed NO production from RAW 264.7 cells when compared with induced cells, and has shown good correlation with antioxidant assays. Along these lines, we identified one member of the Sophora family (*S. flavescens*) that has been shown to arrest the cell cycle and inhibit angiogenesis by downregulating the expression of VEGF [14]. Our results suggest that compounds present in the SEA extract can have powerful physiological effects that make them useful as phytomedicine. However, to date, there were no such documented secondary metabolites

Fig. 5a,b Pictographical representation of root mean squared deviations (RMSDs). **a** RMSD for VEGFR1 with maackiaian (blue) and axitinib (red). **b** RMSD for VEGFR2 with funiculosin (green), maackiaian (blue) and axitinib (red)



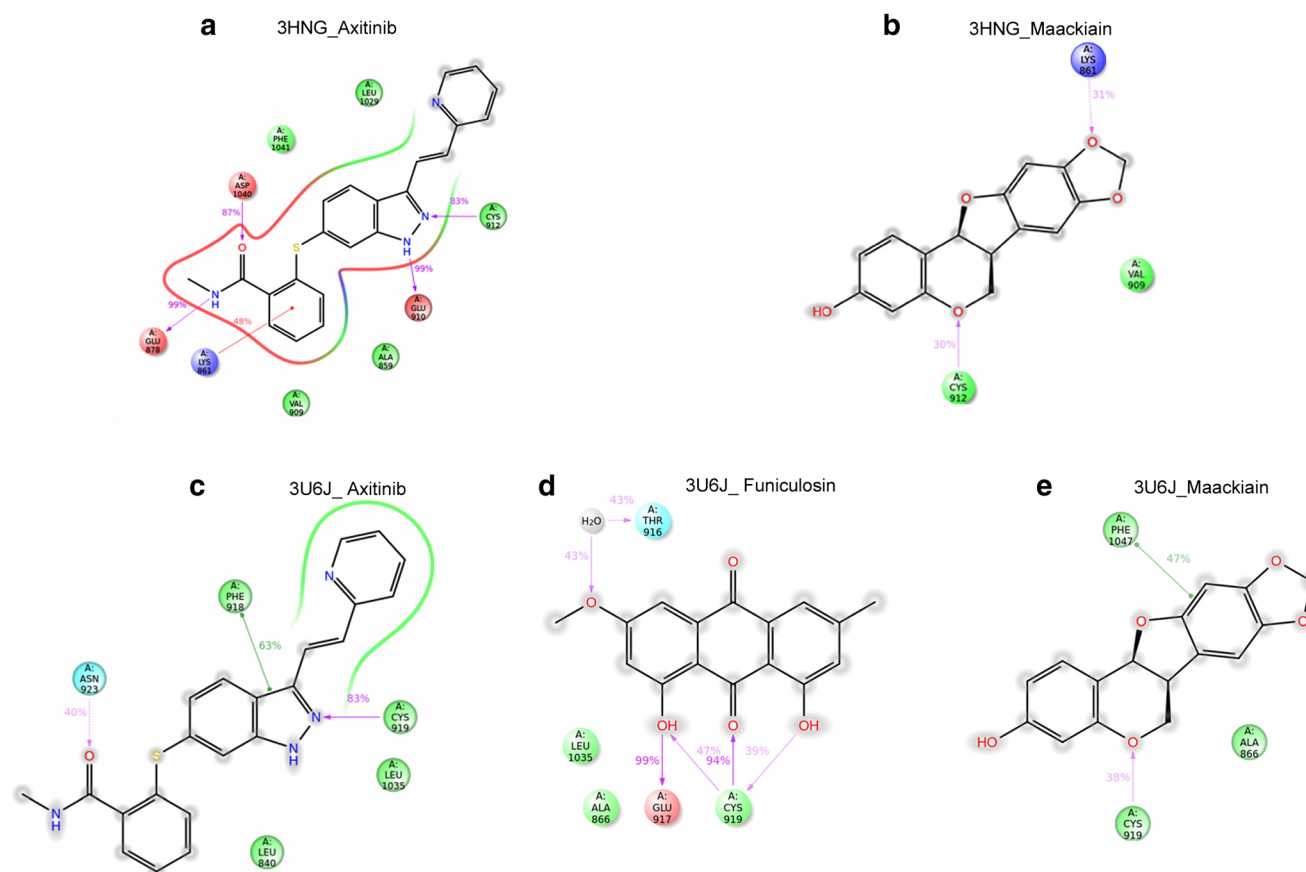


Fig. 6a–e Percentage of compound interactions with amino acid residues in the molecular dynamics (MD) simulations study. **a** Interactions of axitinib in the binding pocket of VEGFR1. **b** Interactions of maackiaïn

in the binding pocket of VEGFR2. **c** Interactions of axitinib in the binding pocket of VEGFR2. **d** Interactions of funiculosin in the binding pocket of VEGFR2. **e** Interactions of maackiaïn in the binding pocket of VEGFR2

from *S. interrupta* or allied species. To evaluate the anti-angiogenic activity of SEA extract, a CAM assay was performed. The development of avascular zone, or a zone of inhibition, at the site of application is considered indicative of anti-angiogenesis. Our results suggest that SEA extract markedly inhibited the growth of blood vessels, and had angiogenesis-inhibiting activity similar to that of cisplatin.

In the search of anti-angiogenic compounds from *S. interrupta*, methods like GC-MS and computational techniques can be used to understand protein–ligand interactions at the atomic level. The presence of 34 compounds was reported from GC-MS analysis, had have begun to be interpreted. For example, a thermopsine compound highly responsible for antioxidant activity, and 1-dodecanol were reported to have antiinflammatory properties. Computational methodologies have become a crucial component in drug discovery approaches, from target identification to lead development. The best hits obtained after docking studies were calculated using the QikProp module to access their pharmacological properties [35]. Both molecules maackiaïn and funiculosin did not violate

Lipinski’s rule-of-five and other described properties. Based on the docking results, a cysteine amino acid in the active pocket of both the receptors was seen to have great affinity towards the lead molecules. We used MD simulations to examine the stability of some compounds in the extract when bound to VEGF receptors. Interestingly, during the total simulation time period, the H-bond observed in the VEGFR1–maackiaïn complex after docking vanished in dynamic simulations, and new interactions were observed with Lys 861 and Cys 912 residues, whereas in the VEGFR1– axitinib complex, the interactions before and after MD simulations were similar. Low deviations and fluctuations were observed, proving the stability of the molecules against VEGFR1.

The VEGFR2–funiculosin complex showed the same type of interactions before and after MD simulations. The interaction profile of the VEGFR2–maackiaïn complex showed a H-bond with Cys 919 that was not observed in the initial frames of the simulation. Axitinib forms H-bonds with Cys 919 and Lys 828 before simulations, and after MD simulation we observed interaction with Cys 919 and Asn 923, but the interaction with Lys 838 disappeared by forming a new interaction

with residue Asn 923; this was due to the conformational changes in the molecule.

From the docking scores, it was clear that the metabolites showed better affinity towards VEGFR1 and VEGFR2. MD simulations gave good results but the H-bonding interaction networks of these high active molecules (maackiain and funiculosin) were contradictory to previous observations since the percentages of interactions were very low when compared with the standard.

From this it was evident that, even though the H-bond interaction percentages of maackiain and funiculosin were low when compared to that of axitinib, high binding energies were observed. The energies (van der Waals, coulombs, torsions, angle energies) of these compounds have compensated for the H-bond energy, due to which the metabolites have higher affinity. The consolidated result from the computational analysis was that maackiain and funiculosin showed good results and may have similar activity when compared to axitinib.

We confirmed the cytotoxicity of SEA extract using brine shrimp as an *in vivo* model. This well-known model is similar to mouse models, and the results obtained with brine shrimp (Fig. S4) have been found to correlate well with acute oral toxicity data obtained in rodents and humans [36]. These results suggest that the formation of funiculosin and maackiain complexes may strongly and selectively inhibit VEGFR2 and thereby inhibit angiogenesis. Plant compounds with similar/identical interaction patterns to commonly used anti-angiogenic drugs such as resveratrol and other anti-angiogenic compounds have been identified; axitinib from traditional Korean medicine was used as a reference compound [37].

Conclusions

The present research study demonstrated that the root ethyl acetate extract of *S. interrupta* Bedd, has good free radical scavenging properties against DPPH and ABTS. The *in vitro* antiinflammatory activity on RAW 264.7 cells was shown to significantly reduce NO production without having any cytotoxic effect. The formation of new blood vessels in CAM models was also inhibited with SEA extract within acceptable ranges. GC-MS analysis identified 34 bioactive compounds that possess many biological roles, such as anticancer, antioxidant, etc. Molecular docking studies highlighted two molecules (funiculosin and maackiain) showing better interactions with VEGFR1 and VEGFR2 proteins. The results of MD simulations of the lead molecules were significant and stable. Thus, based on the results presented, it can be concluded that these bioactive compounds may act as good inhibitors for VEGFRs. In future, derivatives of

S. interrupta may be developed for VEGFR inhibitors and therapeutic agents against cancers.

Acknowledgments This work was partly supported by a grant to M.B. from the Department of Biotechnology, Government of India. The authors thank Dr. S.V. Saradhi, the head of the Department of Biotechnology, for his continuous support; Dr. R. S. Reddy for providing a UV-vis spectrophotometer; and Tayi Narasimharao of Laila Nutraceuticals for helpful discussions on the brine shrimp lethality assay. We also thank Mohanacharyulu, Associate Professor in English for his extreme care with language.

Compliance with ethical standards

Conflict of interest All authors declare that there are no conflicts of interest.

References

- Ribatti D, Crivellato E (2012) “Sprouting angiogenesis”, a reappraisal. *Dev Biol* 372(2):157–165. doi:10.1016/j.ydbio.2012.09.018
- Ono M (2008) Molecular links between tumor angiogenesis and inflammation: inflammatory stimuli of macrophages and cancer cells as targets for therapeutic strategy. *Cancer Sci* 99(8):1501–1506. doi:10.1111/j.1349-7006.2008.00853.x
- Hanahan D, Coussens LM (2012) Accessories to the crime: functions of cells recruited to the tumor microenvironment. *Cancer Cell* 21(3):309–322. doi:10.1016/j.ccr.2012.02.022
- Kobayashi H, Lin PC (2005) Angiopoietin/Tie2 signaling, tumor angiogenesis and inflammatory diseases. *Front Biosci* 10:666–674
- Smolle E, Taucher V, Pichler M, Petru E, Lax S, Haybaeck J (2013) Targeting signaling pathways in epithelial ovarian cancer. *Int J Mol Sci* 14(5):9536–9555. doi:10.3390/ijms14059536
- Bhojani N, Jeldres C, Patard J-J, Perrotte P, Suardi N, Hutterer G, Patenaude F, Oudard S, Karakiewicz PI (2008) Toxicities associated with the administration of sorafenib, sunitinib, and temsirolimus and their management in patients with metastatic renal cell carcinoma. *Eur Urol* 53(5):917–930
- Wenger JB, Santos N, Liu Y, Dallas J, Subbiah S, Hochwald S, Huang EH, Dang DT, Allegra CJ, Luesch H (2011) Can we develop effective combination antiangiogenic therapy for patients with hepatocellular carcinoma? *Oncol Rev* 5(3):177–184
- Johnson BF, Clay TM, Hobeika AC, Lysterly HK, Morse MA (2007) Vascular endothelial growth factor and immunosuppression in cancer: current knowledge and potential for new therapy. *Expert Opin Biol Ther* 7(4):449–460. doi:10.1517/14712598.7.4.449
- Vithya T, Kavimani S, Raj Kapoor B, Alhasjajju K, Premakumari K (2013) *In vitro* antioxidant activity of *Sophora interrupta* by ABTS and hydrogen peroxide method. *J Pharm Res* 1(3):233–234
- Mathi P, Nikhil K, Ambatipudi N, Roy P, Bokka VR, Botlagunta M (2014) *In vitro* and *in silico* characterization of *Sophora interrupta* plant extract as an anticancer activity. *Bioinformation* 10(3):144–151. doi:10.6026/97320630010144
- Hemamalini K, Sathya S (2013) Hepatoprotective activity of *Sophora interrupta* and *Holoptelea integrifolia* against carbon tetrachloride induced hepatotoxicity in rats. *Int J Biol Pharm Allied Sci* 2(1):80–89
- Kumar PS, Sandhya S, Rao K, Banji D, Krishna PM, Rajeshwar T (2011) Pharmacognostical studies and preliminary phytochemical investigations on roots of *Sophora interrupta* Bedd., Fabaceae. *J Phyto* 3(9):42–47

13. Hemamalini K, Bhargav A (2013) Evaluation of phytochemical and pharmacological activity of methanolic extract of *Sophora interrupta*. Indo Am J Pharma Res 3(8):6381–6390
14. Zhang XL, Cao MA, Pu LP, Huang SS, Gao QX, Yuan CS, Wang CM (2013) A novel flavonoid isolated from *Sophora flavescens* exhibited anti-angiogenesis activity, decreased VEGF expression and caused G₀/G₁ cell cycle arrest in vitro. Pharmazie 68(5):369–375
15. Proestos C, Lytoudi K, Mavromelanidou O, Zoumpoulakis P, Sinanoglou V (2013) Antioxidant capacity of selected plant extracts and their essential oils. Antioxidants 2(1):11–22. doi:10.3390/antiox2010011
16. Raschke WC, Baird S, Ralph P, Nakoinz I (1978) Functional macrophage cell lines transformed by Abelson leukemia virus. Cell 15(1):261–267. doi:10.1016/0092-8674(78)90101-0
17. Srisook K, Han S-S, Choi H-S, Li M-H, Ueda H, Kim C, Cha Y-N (2006) CO from enhanced HO activity or from CORM-2 inhibits both O₂⁻ and NO production and downregulates HO⁻¹ expression in LPS-stimulated macrophages. Biochem Pharmacol 71(3):307–318
18. Foubert K, Breynaert A, Theunis M, Van Den Bossche R, De Meyer GR, Van Daele A, Faizal A, Goossens A, Geelen D, Conway EM, Vlietinck A, Pieters L, Apers S (2012) Evaluation of the anti-angiogenic activity of saponins from *Maesa lanceolata* by different assays. Nat Prod Commun 7(9):1149–1154
19. Lee J, Majumder S, Chatterjee S, Muralidhar K (2011) Inhibitory activity of the peptides derived from buffalo prolactin on angiogenesis. J Biosci 36(2):341–354
20. Available at: <http://www.rcsb.org/pdb/explore/explore.do?structureId=3U6J> Accessed 17 April 2014, and <http://www.rcsb.org/pdb/explore/explore.do?structureId=3HNG> Accessed 17 April 2014
21. Khokra SL, Monga J, Husain A, Vij M, Saini R (2013) Docking studies on butenolide derivatives as Cox-II inhibitors. Med Chem Res 22(11):5536–5544. doi:10.1007/s00044-013-0511-x
22. Banks JL, Beard HS, Cao Y, Cho AE, Damm W, Farid R, Felts AK, Halgren TA, Mainz DT, Maple JR, Murphy R, Philipp DM, Repasky MP, Zhang LY, Berne BJ, Friesner RA, Gallicchio E, Levy RM (2005) Integrated Modeling Program, Applied Chemical Theory (IMPACT). J Comput Chem 26(16):1752–1780. doi:10.1002/jcc.20292
23. Williams AJ (2011) Chemspider: a platform for crowdsourced collaboration to curate data derived from public compound databases. Collaborative computational technologies for biomedical research. Wiley, New York, pp 363–386. doi:10.1002/9781118026038.ch22
24. Sastry GM, Inakollu VS, Sherman W (2013) Boosting virtual screening enrichments with data fusion: coalescing hits from two-dimensional fingerprints, shape, and docking. J Chem Inf Model 53(7):1531–1542. doi:10.1021/ci300463g
25. Srinivasan P, Chella Perumal P, Sudha A (2014) Discovery of novel inhibitors for Nek6 protein through homology model assisted structure based virtual screening and molecular docking approaches. Sci World J 2014:967873. doi:10.1155/2014/967873
26. Friesner RA, Banks JL, Murphy RB, Halgren TA, Klicic JJ, Mainz DT, Repasky MP, Knoll EH, Shelley M, Perry JK, Shaw DE, Francis P, Shenkin PS (2004) Glide: a new approach for rapid, accurate docking and scoring. 1. Method and assessment of docking accuracy. J Med Chem 47(7):1739–1749. doi:10.1021/jm0306430
27. Halgren TA, Murphy RB, Friesner RA, Beard HS, Frye LL, Pollard WT, Banks JL (2004) Glide: a new approach for rapid, accurate docking and scoring. 2. Enrichment factors in database screening. J Med Chem 47(7):1750–1759. doi:10.1021/jm030644s
28. Palakurti R, Sriram D, Yogeewari P, Vadrevu R (2013) Multiple e-Pharmacophore modeling combined with high-throughput virtual screening and docking to identify potential inhibitors of β -Secretase (BACE1). Mol Info 32(4):385–398. doi:10.1002/minf.201200169
29. Guo Z, Mohanty U, Noehre J, Sawyer TK, Sherman W, Krilov G (2010) Probing the alpha-helical structural stability of stapled p53 peptides: molecular dynamics simulations and analysis. Chem Biol Drug Des 75(4):348–359. doi:10.1111/j.1747-0285.2010.00951.x
30. Stein SE (1999) An integrated method for spectrum extraction and compound identification from gas chromatography/mass spectrometry data. J Am Soc Mass Spectrom 10(8):770–781. doi:10.1016/s1044-0305(99)00047-1
31. Savjani KT, Gajjar AK, Savjani JK (2012) Drug solubility: importance and enhancement techniques. ISRN Pharm 2012:195727. doi:10.5402/2012/195727
32. Cui X, Wang Y, Kokudo N, Fang D, Tang W (2010) Traditional Chinese medicine and related active compounds against hepatitis B virus infection. Biosci Trends 4(2):39–47
33. Sakarkar D, Deshmukh V (2011) Ethnopharmacological review of traditional medicinal plants for anticancer activity. Int J Pharma Tech Res 3(1):298–308
34. Kim Y, Lee J (2014) Anti-inflammatory activity of capsaicin and dihydrocapsaicin through heme oxygenase-1 induction in raw264.7 macrophages. J Food Biochem 38 (4):n/a-n/a. doi:10.1111/jfbc.12064
35. Suomalainen P, Johans C, Soderlund T, Kinnunen PK (2004) Surface activity profiling of drugs applied to the prediction of blood–brain barrier permeability. J Med Chem 47(7):1783–1788. doi:10.1021/jm0309001
36. Lagartoparra A (2001) Comparative study of the assay of and the estimate of the medium lethal dose (LD₅₀ value) in mice, to determine oral acute toxicity of plant extracts. Phytomedicine 8(5):395–400. doi:10.1078/0944-7113-00044
37. Seo EJ, Kuete V, Kadioglu O, Krusche B, Schroder S, Gretten HJ, Arend J, Lee IS, Efferth T (2013) Antiangiogenic activity and pharmacogenomics of medicinal plants from traditional Korean medicine. Evid Based Complement Alternat Med 2013:131306. doi:10.1155/2013/131306